Modelling of Heat Transfer for Droplet Condensation in Mixed Convective Duct Flow

Christian Brückner[1(✉)], Andreas Westhoff[1], and Claus Wagner[1,2]

[1] German Aerospace Center (DLR), Institute of Aerodynamics and Flow Technology, Bunsenstr. 10, 37073 Göttingen, Germany
christian.brueckner@dlr.de

[2] Technische Universität Ilmenau, Institute of Thermodynamics and Fluid Mechanics, Helmholtzring 1, 98693 Ilmenau, Germany

Abstract. Temperature and humidity measurements are conducted in mixed convective humid-air duct flow with condensation. The latent and total heat transfer during the experiment are determined through the thermal balance for inlet temperatures from 27.5 °C to 35.5 °C, relative humidities from 30% to 55% and at four Reynolds numbers (2000–8000). The experimental results are compared with a heat transfer model from the literature. Adjusted in terms of the geometry and surface properties, the model shows partial agreement for the cases with forced convection but has to be further adjusted regarding the influence of thermal convection.

Keywords: Condensation · Duct flow · Heat transfer

1 Condensation

The widespread use of condensation heat transfer in the energy sector and in air conditioning systems has led to an increased interest in the development of prediction models. For more than 100 years, formulations of models have been investigated by many researchers in order to describe heat transfer in relation to thermal conditions, geometry, material properties and flow conditions [7].

Especially the presence of non-condensable gas (ncg) fractions complicates or even impedes the predictability of the heat transfer as it leads to local accumulation of these gas fractions at the condensate interface. This in turn results in the formation of a diffusion layer and to additional resistance for the latent

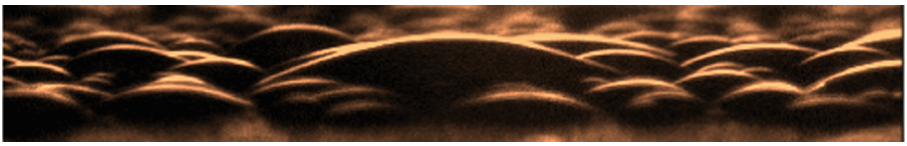

Fig. 1. Condensate droplets on the cooled wall

A. Dillmann et al. (Eds.): STAB/DGLR Symposium 2020, NNFM 151, pp. 461–471, 2021.
https://doi.org/10.1007/978-3-030-79561-0_44

Nomenclature

Dimensionless Numbers

Gr	Grashof	$\frac{g\,\beta(T_{in}-T_w)d_h^3}{\nu_{air}^2}$
Nu	Nusselt	$\frac{h\,d_h}{\lambda_{air}}$
Pr	Prandtl	$\frac{\eta c_p}{\lambda_{air}}$
Re	Reynolds	$\frac{U d_h}{\nu}$
Ri	Richardson	$\frac{Gr}{Re^2}$
Sc	Schmidt	$\frac{\nu}{D}$

Symbols

A	area
B_i	mass transfer driving force
C	correction factor
c_p	heat capacity
C_D	drag coefficient
D	diffusion coefficient
d_h	hydraulic diameter
F	force
g	gravitational acceleration
H	(duct) height
h	heat transfer coefficient
h_v	heat of evaporation
L	duct length
$\dot{m}$	mass flow
$\dot{q}$	heat flux
r	radius
T	temperature
u	bulk velocity
$\dot{V}$	volume flow
W	duct width
w	mass fraction

β	thermal expansion coefficient
γ	surface tension
η	dynamic viscosity
λ_{air}	thermal conductivity
ν	kinematic viscosity
θ	contact angle
ζ	contact line radius

Subscripts

a	ambient
air	airflow
D	drag
d	droplet
dp	dewpoint
g	gravity
i	condensate interface
in	inlet
lat	latent heat transfer
nc	non-condensable fraction
vo	outlet
ow	opposite wall
sen	sensible heat
s	surface tension
test	test section
t	total
water	water fraction
w	cooled wall
x,0	begin of test section
x,L	end of test section
x,m	mean of test section

heat transfer. In case of very high fractions of ncg, i.e. humid air, the dominant factor changes from a local depletion of vapour in the diffusion layer to convective mass transfer in the humid air, which is determined by the flow conditions. Through manipulation of the condensate substrate surface towards hydrophobic behaviour and for small rates of condensation on other surfaces, droplet condensation is observed. A sample result of droplets on a condensate substrate is shown in Fig. 1. The size of such droplets is too small to have a direct effect on the wall-bounded flow. However, the increased surface area compared to a plain wall or condensate film adds to the latent heat transfer [2].

Danilo et al. analysed the condensation heat transfer in turbulent convective humid air flow [3]. In their horizontal experiment condensate mass is increased linearly until the critical droplet size is reached. When agglomeration of the droplets starts and a continuous film forms, the global heat transfer stagnates with a reduced amount of convective heat transfer. The latent heat transfer depends on the humidity level and dominates the global heat transfer at high relative humidities. For very small droplets, no impact on the convective heat transfer was observed. Additionally, different humidity levels had no significant impact on the convective heat transfer at similar drop sizes and distributions.

1.1 Model Despcription

Eimann et al. [5] used the diffusion layer model of Peterson et al. [8] and Caruso et al. [2] and developed the model *further* based on their own condensation experiment. The experiment consists of a horizontally oriented rectangular duct with a cross section of 12 mm × 32 mm in which a vertical cooled plate of 9 mm × 6 mm is installed. The cooled plate has the additional function of a heat flux sensor in order to directly record the total heat flux resulting from the latent and sensible heat. The heat flux is recorded in a Reynolds number range $3000 < Re < 22000$ for 36 °C to 55 °C for 36 % to 55% relative humidity.

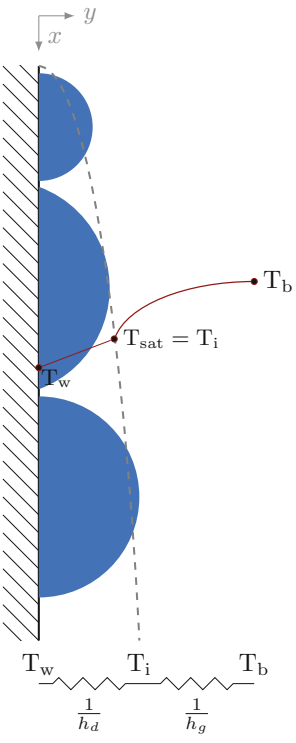

Fig. 2. Scheme of the droplet condensation

The fundamental approach to the heat transfer for dropwise condensation is considered to be a cascade of thermal resistances, the reciprocal of which are the separate heat transfer coefficients. In Fig. 2 the temperature profile between the bulk temperature T_b, the droplet interface temperature T_i and the wall temperature T_w as well as the separate thermal resistances for the droplet $1/h_d$ and the gas-liquid interface $1/h_g$ are illustrated schematically. The sum of the thermal resistances gives the total heat transfer coefficient h_t

$$h_t = \left[\frac{1}{h_d} + \frac{1}{h_g}\right]^{-1}. \tag{1}$$

The individual heat transfer coefficients h_g and h_d are determined with the help of the experimentally obtained total heat flux $\dot{q}_t$ and the temperature of the condensate interface T_i. The partial heat fluxes are determined by the local thermal balance

$$\dot{q}_t = h_t(T_b - T_w) = h_d(T_i - T_w) = h_g(T_b - T_i). \tag{2}$$

Eimann et al. [4] used thermographic imaging to determine the interface temperature for a given droplet size and derived a temporal and spatially

averaged formulation for h_d that they extended for the parameter range of $2000 < Re < 21400$

$$h_d = \frac{0.347 Re_b}{1 + 1.75 \exp(-330.5 B_i)} \quad \text{with} \quad B_i = \ln\left(\frac{w_{nc,i}}{w_{nc,b}}\right). \tag{3}$$

Here, B_i denotes the driving force for the mass transfer with w_{nc} being the mass fraction of non-condensable gas fraction at the interface and in the bulk, respectively. To calculate the mass fraction at the interface, saturation at the interface is assumed and the Gibbs-Dalton law is applied as formulated by Caruso and Di Vitale Maio [2].

The heat transfer coefficient at the gas-liquid interface h_g is derived from the corresponding Nusselt number Nu_g, which in turn is the sum of sensible and latent Nusselt numbers

$$Nu_g = C(Nu_{sen} + Nu_{lat}). \tag{4}$$

Both Nusselt numbers are determined using $Nu - Re$ relations from the literature for duct flows. The correction factor C is introduced to compensate for the influence of the droplets. It is correlated with the critical droplet radius r_{max} for each case and defined as a linear function for $0.2 < r_{max} < 1.61$ mm [5].

Additionally, an iterative procedure is introduced to predict the total heat transfer coefficient based on a measured Reynolds number Re, bulk temperature T_b, wall temperature T_w and non-condensable mass fraction in the bulk $w_{nc,b}$.

The objective of this work is to test the model approach of Eimann et al. against the experimentally determined heat fluxes of a vertical duct flow with condensation on a cooled wall. The comparison of experimental and model data is discussed in terms of the transfer to a larger condensation surface as well as regarding the influence of thermal convection on the heat transfer.

2 Experimental Setup

The experiments are performed in a vertically oriented, differentially cooled duct with a rectangular cross section. The cross section of the duct is 50×533 mm and the cooled surface of the test section has a length of 2.05 m [1]. The temperatures of the duct are controlled with a water-cooled aluminium sheet on one side and a four-zone electrically heated aluminium sheet to achieve isothermal conditions on either side. A sketch of the duct setup is shown in Fig. 3. Upstream of the test section, the inlet section ensures a well-defined, homogenous inflow and downstream of the test section, an outlet section ensures an undisturbed flow in the test section. The aspect ratio of 10.66:1 is chosen to minimize the influence of the side walls, thermal or through the boundary layer. The temperature of the heated wall T_{ow} is equal to the inlet temperature T_{in} in order to minimize the heat flux at this side of the duct.

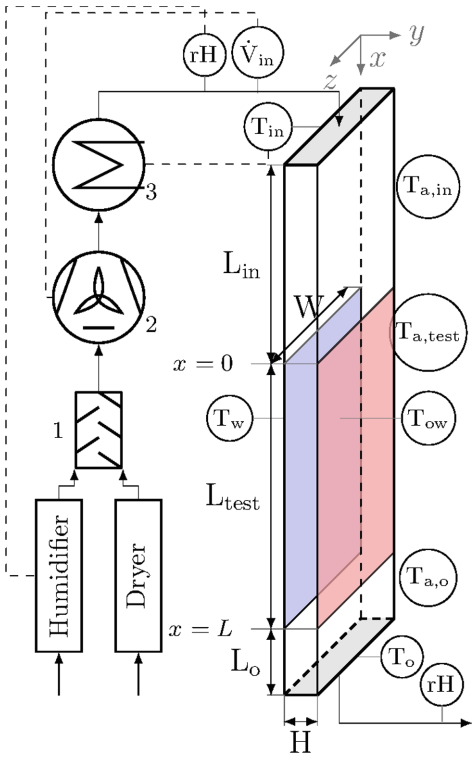

Fig. 3. Process flow diagram of the vertical duct with isothermally cooled wall (T_w, blue) and isothermally heated opposite wall (T_{ow}, red). (1) static mixer; (2) radial fan; (3) heat exchanger

The measurements are conducted for $2000 < Re < 8000$, an inlet temperature range of 27.5 °C to 35.5 °C and a relative humidity range of 30 % to 50% at the inlet. In total, 35 data points are collected. The temperature difference between cooled wall T_w and inlet temperature T_{in} was set to 26.5 K in all experiments to keep Gr in the order of 2.4×10^6.$Further, Pr$ and Sc are at near constant levels at 0.75 and 0.65, respectively. With a variation of Re at constant Gr, the Ri yields 0.62 to 0.033.

2.1 Thermal Balance

To determine the heat flux of the experiment, the observed temperatures T_{in}, T_o, T_w, the dew point temperatures $T_{dp,in}$, $T_{dp,out}$ and the air mass flow $\dot{m}_{air}$ are time-averaged and the thermal balance is

$$\dot{q}_{air} = \dot{q}_t + \dot{q}_{lat} + \dot{q}_a, \tag{5}$$

with the contributing total heat flux from fluid to the wall

$$\dot{q}_t = h_t \mathrm{L_{test}} \mathrm{W} (T_{x,m} - T_w), \tag{6}$$

heat flux due to the change in heat capacity of the air

$$\dot{q}_{air} = \dot{m}_{air}(c_{p,in}T_{x,0} - c_{p,o}T_{x,L}), \tag{7}$$

the latent heat flux, directly calculated from the condensate mass

$$\dot{q}_{lat} = \dot{m}_c h_v, \tag{8}$$

and the ambient heat flux through the side walls

$$\dot{q}_a = h_{a,t} 2\mathrm{HL}_{\mathrm{test}}(T_{x,m} - T_{a,t}). \tag{9}$$

The thermal balance is solved analytically with the idealisation of a spatially averaged heat transfer coefficient h_t for the total heat transfer from the fluid to the wall. The heat transfer coefficient h_t and the mean temperature $T_{x,m}$ are then determined by iteration to match the observed outlet temperature [10]. All material properties are considered at the determined mean temperature $T_{x,m}$ (Fig. 3).

2.2 Adjustment of the Droplet Force Balance

Since the air flow in this experiment is in vertical direction, the contribution to the force balance for the droplets has to be adjusted compared to the horizontal flow in the Eimann model.

$$F_g + F_s + F_D = 0 \tag{10}$$

The gravitational force F_g and the drag force F_d act in the same direction, while the surface tension force F_s keeps the droplet on the wall. All three forces depend on the droplet radius r [9]:

$$F_g = \varrho_{water}\, V(r)\, g \tag{11}$$

$$F_s = -\gamma \int_0^{2\pi} \zeta(r) \cos\theta \cos\phi \, d\phi \tag{12}$$

$$F_D = \frac{1}{2} C_D\, \varrho_{air}\, u^2\, A_{proj}(r) \tag{13}$$

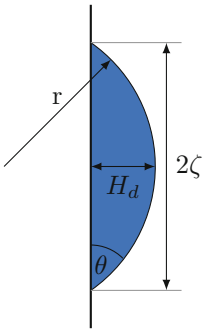

Fig. 4. Vertical projection of the droplet geometry with $\theta < 90°$

Due to contact angles significantly deviating from 90°, the volume $V(r)$ is calculated for a spherical cap rather than a half sphere

$$V = \frac{\pi}{3} r^3 (2 + \cos\theta)(1 - \cos\theta)^2. \tag{14}$$

The vertical projection area $A_{proj}(r)$ of a droplet can be simplyfied to a circle segment

$$A_{proj} = \frac{r^2}{2} \left(2\,\bar{\theta} - \sin(2\,\bar{\theta})\right). \tag{15}$$

The mean contact angle $\bar{\theta}$ has a limited validity and can only be used for small deformations due to gravity.

3 Results

The first step of the model approach was to identify the force balance of the droplet in order to determine the critical droplet radius r_{max}. In the experiment, an otherwise untreated anodized aluminium plate was used as condensation surface. The contact angle θ was measured to be $63.3° \pm 15°$ at 18 positions of the surface in a horizontal position. Three sample droplets are shown in Fig. 5 revealing the large spread of contact angles at different positions of the condensation surface. The high variance comes with the large area as well as the long-term use of the aluminium plate and is seen as a more realistic, commonplace condensation surface.

The maximum radii for the different Re as calculated via the force balance and determined experimentally are shown in Fig. 6 for all cases. The force balance gives a similar radius of 3.6 mm for all cases. In the experiment, the maximum radius observed was smaller with values from 2 mm to 2.8 mm. Since the contact angle is significantly smaller than 90° for single droplets and further distorted through coalescence, this difference in radius does not translate into a major difference of the droplet forces. It does, however, significantly impact Eimanns correction factor C, which is only defined up to 1.61 mm and will be discussed further with the total heat transfer.

The experiment provides a direct method of calculating the total condensate mass using the thermal balance. The comparison of the measured latent heat and the projected latent heat by the correlation taken from the VDI Heat Atlas [6] is shown in Fig. 7 in case of an inlet temperature of $T_{in} = 31.5\,°\mathrm{C}$. For the lower Re, the predicted latent heat transfer is too small (Fig. 7a and 7b). While the correlation does consider the transition from laminar to turbulent flow, it does not consider the additional influence of thermal convection introduced to the flow by the cooled wall.

Since the temperature difference, and therefore the Grashof number, is constant for all cases, the influence of the thermal convection is larger at lower Re, where the forced convection is not yet dominant ($0.13 < Ri < 0.62$). In this case, the thermal convection leads to an increased latent heat transfer, probably caused by the accelerated air close to the wall. Due to continuity, the acceleration in the boundary layer leads to a deceleration in the bulk flow and thus to a longer dwell time of the humid air. To compensate for the thermal convection, a modified latent Nusselt number was formed using Ri

$$Nu^*_{lat} = (1 + C_{Ri}\, Ri) Nu_{lat} \quad \text{with}\, C_{Ri} = 3.012. \tag{16}$$

The correction factor $C_{Ri} = 3.012$ fits the experiment data best.

Fig. 5. Various contact angle samples on horizontal surface

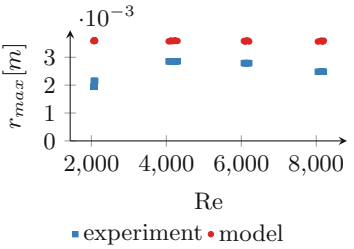

Fig. 6. Critical droplet radius r_{max} over the Re for all cases

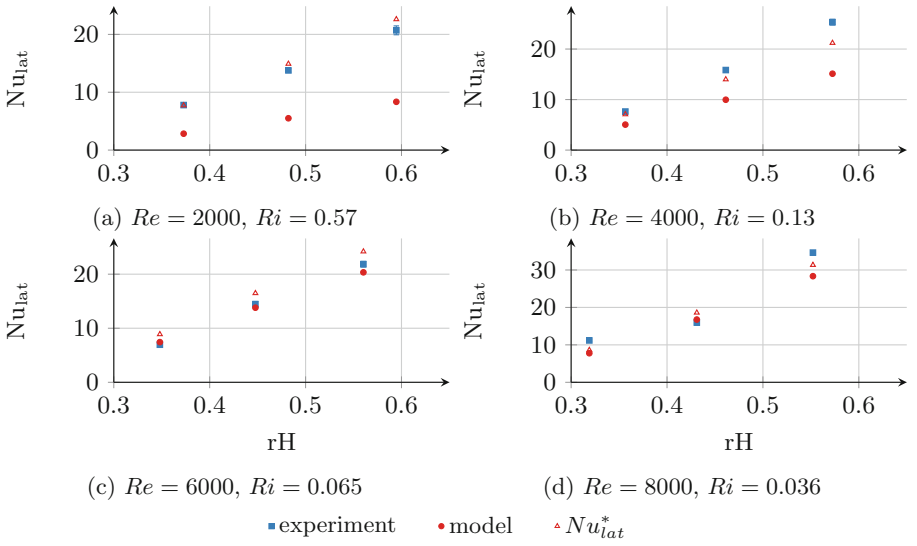

Fig. 7. Nusselt number for latent heat transfer over relative humidity for Re at varying velocities at $T_{in} = 31.5\,^{\circ}\mathrm{C}$. The relative uncertainty of Nu is at approx. 3.5% (still inside the square mark)

For the highest Re, the influence of thermal convection is very small ($Ri = 0.036$) and thus, the prediction fits reasonably well with the measured latent heat transfer (Fig. 7c and 7d). In all four cases, the prediction is more accurate for the lower relative humidity. This might be an indicator, that even for these comparably low relative humidities, the fog formation has a relevant influence that has to be taken into account.

Figure 8 shows the Nusselt number for the total heat flux from the humid air to the cooled wall for the experiment and the model in two configurations. The first uses the critical radius observed in the experiment, and the second uses the droplet height H_d instead. For the observed contact angles, the droplet

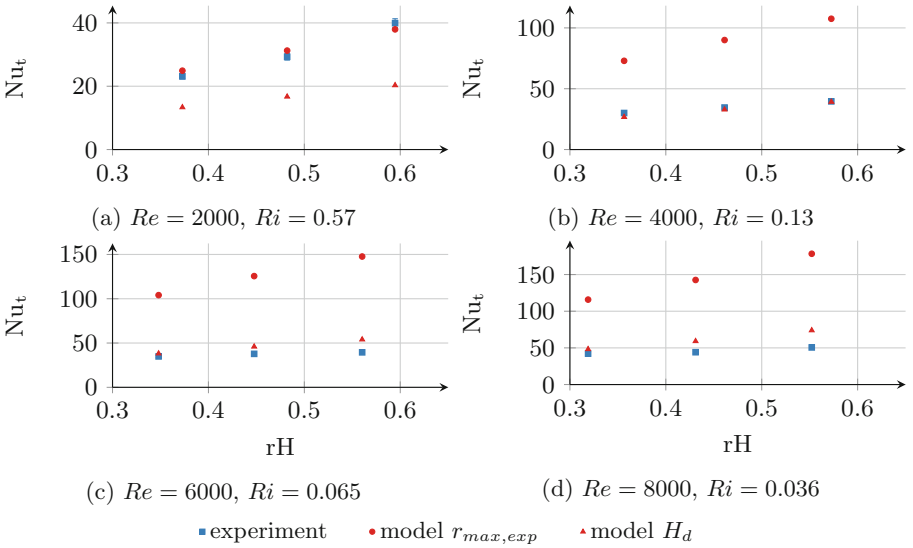

Fig. 8. Nusselt number for total heat transfer over relative humidity for Re at varying velocities at $T_{in} = 31.5\,^{\circ}\mathrm{C}$

height and radius diverge significantly compared to the idealised 90° originally used in the model. Since the correction factor is intended for the deviation from a homogenous film, the droplet height appears to be a reasonable replacement. For Re 2000 in Fig. 8a, the model prediction using the critical radius shows reasonable agreement. For the other cases Re 4000, Re 6000 and Re 8000 (Fig. 8b, 8c and 8d), the predicted heat transfer amounts to two or three times the value of the experiment. Using the model with the droplet height results in much better agreement in these cases, even though the model still overpredicts the Nusselt number at Re 6000 and Re 8000. In combination with the information about the latent heat transfer, the deviation at Re 6000 and Re 8000 shows that the predicted sensible heat is too high, especially for the higher relative humidities. The Re 2000 case adjusted to the missing latent heat would still not agree better with the observed droplet radius, but again the influence of thermal convection is not accounted for by the model.

Based on these results, the droplet height is a more suitable substitute for the critical radius in cases with contact angles θ smaller than 90°

$$H_{d,max} = r_{max}\,(1 - \cos(\bar{\theta})). \tag{17}$$

4 Conclusion

Condensation heat transfer in a mixed convective duct flow has been studied experimentally and the results have been compared to a prediction model for dropwise condensation based on the diffusion layer model. The measurements

show an increase of the latent and sensible heat transfer with increasing relative humidity and humid air velocity. The prediction model was adjusted to the differing experimental geometry and flow direction as well as to the droplet characteristics. The comparison of the latent heat revealed a significant influence of the thermal convection and a correction based on the Richardson number Ri is introduced.

The maximum droplet radius as the core parameter in the prediction model was replaced by the corresponding droplet height in order to adjust the model to be used with contact angles smaller than 90°. While this still leads to an over-prediction of the sensible heat transfer, especially for higher relative humidities, it shows reasonable agreement with the experimental data. The remaining over-prediction is attributed to the depletion of water vapour over the condensation surface. This effect has to be further analysed in the future in order to find an equivalent droplet height that factors in the effect of both, surface and condensation rate.

Acknowledgement. The authors like to thank Annika Köhne and Konstantin Niehaus for their contribution to this paper.

References

1. Brückner, C., Bahavar, P., Westhoff, A., Wagner, C.: Reynolds number dependency of the heat and mass transfer in mixed convective duct flow with condensation at a cooled wall. In: Dillmann, A., Heller, G., Krämer, E., Wagner, C., Tropea, C., Jakirlić, S. (eds.) DGLR 2018. NNFMMD, vol. 142, pp. 523–532. Springer, Cham (2020). https://doi.org/10.1007/978-3-030-25253-3_50. ISBN 978-3-030-25253-3
2. Caruso, G., Di Maio, D.V.: Heat and mass transfer analogy applied to condensation in the presence of noncondensable gases inside inclined tubes. Int. J. Heat Mass Transfer **68**(1–3), 401–414 (2014). https://doi.org/10.1016/j.ijheatmasstransfer.2013.09.049. ISSN 00179310
3. Danilo, S., Dominique, C., Frédéric, P.: Experimental dropwise condensation of unsaturated humid air - influence of humidity level on latent and convective heat transfer for fully developed turbulent flow. Int. J. Heat Mass Transfer **102**, 846–855 (2016). https://doi.org/10.1016/j.ijheatmasstransfer.2016.06.001. ISSN 00179310
4. Eimann, F., Zheng, S., Philipp, C., Fieback, T., Gross, U.: Convective dropwise condensation out of humid air inside a horizontal channel - experimental investigation of the condensate heat transfer resistance. Int. J. Heat Mass Transfer **127**, 448–464 (2018). https://doi.org/10.1016/j.ijheatmasstransfer.2018.08.015. ISSN 00179310
5. Eimann, F., Zheng, S., Philipp, C., Omranpoor, A.H., Gross, U.: Dropwise condensation of humid air - experimental investigation and modelling of the convective heat transfer. Int. J. Heat Mass Transfer **154**, 119734 (2020). https://doi.org/10.1016/j.ijheatmasstransfer.2020.119734. ISSN 00179310
6. Gnielinski, V., et al.: VDI Heat Atlas. VDI Gesellschaft Verfahrenstechnik und Chemieingenieurwesen, 2nd edn (2010). https://doi.org/10.1007/978-3-540-77877-6_94. ISBN 9783540778769
7. Huang, J., Zhang, J., Wang, L.: Review of vapor condensation heat and mass transfer in the presence of non-condensable gas. Appl. Thermal Engi. **89**, 469–484 (2015). https://doi.org/10.1016/j.applthermaleng.2015.06.040. ISSN 13594311

8. Peterson, P.F., Schrock, V.E., Kageyama, T.: Diffusion layer theory for turbulent wapor condensation with noncondensable gases. J. Heat Transfer **115**(4), 998–1003 (1993). https://doi.org/10.1115/1.2911397. ISSN 15288943
9. Sommers, A.D., Ying, J., Eid, K.F.: Predicting the onset of condensate droplet departure from a vertical surface due to air flow-applications to topographically-modified, micro-grooved surfaces. Exp. Thermal Fluid Sci. **40**, 38–49 (2012). https://doi.org/10.1016/j.expthermflusci.2012.01.031. ISSN 08941777
10. Westhoff, A.: Experimental study of heat and mass transfer in convective flows of moist air with droplet condensation as a function of surface roughness and wetting properties. In: Proceedings of the 5th International Conference on Experimental Fluid Mechanics, pp. 692–697 (2018). https://doi.org/10.18726/2018_2. ISBN 978-3-943207-32-3